Chemoselective Synthesis of Folic Acid−Functionalized Magnetite Nanoparticles via Click Chemistry for Magnetic Hyperthermia

Koichiro Hayashi, Makoto Moriya, Wataru Sakamoto, and Toshinobu Yogo*

Division of Nanomaterials Science, EcoTopia Science Institute, Nagoya University Furo-cho, Chikusa-ku, Nagoya 464-8603, Japan

Received November 14, 2008. Revised Manuscript Received February 2, 2009

Folic acid-functionalized Fe_3O_4 nanoparticles (FA-Fe_3O_4 NPs) were synthesized from iron(III) 3-allylacetylacetonate (IAA) through *in situ* hydrolysis and ligand modification, by applying the principle of "click chemistry". The γ-carboxylic acid of FA was successfully bound to the ligand of the Fe_3O_4 NPs without the loss of the α-carboxylic acid group of folic acid (FA), which has an affinity for folate receptors (FRs) expressed on tumor cells. The Fe_3O_4 NPs were monodisperse, and their size was controlled by varying the conditions of IAA hydrolysis. The FA-Fe_3O_4 NPs, which had diameters of 8 nm, exhibited superparamagnetic behavior and a relatively high magnetization at room temperature. The blocking temperature was determined to be 220 K, and the magnetization curve exhibited a remanence of 19 emu/g and a coercivity of 550 Oe at 5 K. The specific absorption rate (SAR) was dependent on the size of the FA-Fe_3O_4 NPs and the strength of the applied magnetic field. The SAR of the 8-nm FA-Fe_3O_4 NPs was 670 W/g in a 230 kHz alternating magnetic field and 100 Oe. The chemoselective surface modification of magnetite particles with FA yielded a novel cancer-targeting system for use in hyperthermia treatment.

Introduction

Magnetic nanoparticles (NPs) have recently attracted considerable attention, because of their applications in diagnostic and therapeutic tools (for example, contrast agents for magnetic resonance imaging,[1] carriers for drug and gene delivery,[2] and agents for magnetic separation,[3] and magnetic hyperthermia[4]). The principle of magnetic hyperthermia is based on the exothermic properties of magnetic materials under the influence of an alternating current (AC) magnetic field; this technique specifically destroys tumors without damaging normal tissues by selective heating the tumor cells. Tumors are more sensitive to heat than normal tissues, and the survival rate of tumors decreases gradually with an increase in temperature up to 42.5 °C, and drastically decreases with further increases in temperature.[5] In addition, tumors are heated more easily than the surrounding normal tissues, because of their poorer vascularization.[6] Therefore, magnetic hyperthermia is a promising cancer thermotherapy.

A superconducting magnet is used to deliver magnetic particles to tumors.[7] When tumor-specific agents are combined with magnetic particles, the latter aggregate on the tumor. To target specific cancer cell lines, monoclonal antibodies immobilized on the surface of the magnetic NPs are used.[8,9] Although antibodies exhibit excellent tumor-binding specificity, their high cost, low availability, and the required difficulties for incubation limit their applications.

Folic acid (FA), which is a water-soluble form of vitamin B, targets tumors in a manner similar to monoclonal antibodies. This is because FA has a high affinity for folate receptors (FRs), which are overexpressed in various types of human tumors but generally are absent in most normal tissues.[10] FA has several advantages over macromolecules (such as monoclonal antibodies) as a tumor-targeting ligand: (1) easy availability; (2) low cost; (3) applicability over a wide range of tumors, such as laryngeal, ovarian, endometrial, colorectal, breast, lung, renal-cell, and neuroendocrine carcinomas;[10−14] (4) ease of cytosolic delivery when combined with magnetic NPs, because the FR-targeting ligand complex can be internalized via endocytosis; and (5) potential for repeated administration, because of its small size, as compared to other targeting ligands. The α-carboxyl group

* Author to whom correspondence should be addressed. Phone: 81-52-789-2750. Fax: 81-52-789-2121. E-mail: yogo@esi.nagoya-u.ac.jp.

(1) Lee, J. H.; Huh, Y. M.; Jun, Y. W.; Seo, J. W.; Jang, J. T.; Song, H. T.; Kim, S.; Cho, E. J.; Yoon, H. G.; Suh, J. S.; Cheon, J. *Nat. Med.* **2007**, *13*, 95.
(2) Yoon, T. J.; Kim, J. S.; Kim, B. G.; Yu, K. N.; Cho, M. H.; Lee, J. K. *Angew. Chem., Int. Ed.* **2005**, *44*, 1068.
(3) Lee, J.; Lee, Y.; Youn, J. K.; Na, H. B.; Yu, T.; Kim, H.; Lee, S. M.; Koo, Y. M.; Kwak, J. H.; Park, H. G.; Chang, H. N.; Hwang, M.; Park, J. G.; Kim, J.; Hyeon, T. *Small* **2008**, *4*, 143.
(4) Mornet, S.; Vasseur, S.; Grasset, F.; Duguet, E. *J. Mater. Chem.* **2004**, *14*, 2161.
(5) Gerweck, L. E. *Radiat. Res.* **1977**, *70*, 224.
(6) Cavaliere, R.; Ciocatto, E. C.; Giovanella, B. C.; Heidelberger, C.; Johnson, R. O.; Margottini, M.; Mondovi, B.; Moricca, G.; Fanelli, A. R. *Cancer* **1967**, *20*, 1351.
(7) Mishima, F.; Takeda, S.; Izumi, Y.; Nishijima, S. *IEEE Trans. Appl. Supercond.* **2007**, *17*, 2303.
(8) Yang, J.; Lee, C. H.; Ko, H. J.; Suh, J. S.; Yoon, H. G.; Lee, K.; Huh, Y. M.; Haam, S. *Angew. Chem., Int. Ed.* **2007**, *46*, 8836.
(9) Huh, Y. M.; Jun, Y. W.; Song, H. T.; Kim, S.; Choi, J. S.; Lee, J. H.; Yoon, S.; Kim, K. S.; Shin, J. S.; Suh, J. S.; Cheon, J. *J. Am. Chem. Soc.* **2005**, *127*, 12387.
(10) Sudimack, J.; Lee, R. J. *Adv. Drug Delivery Rev.* **2000**, *41*, 147.
(11) Sirotnak, F. M.; Tolner, B. *Annu. Rev. Nutr.* **1999**, *19*, 91.
(12) Almadori, G.; Bussu, F.; Navarra, P.; Galli, J.; Paludetti, G.; Giardina, B.; Maurizi, M. *Cancer* **2006**, *107*, 328.
(13) Weitman, S. D.; Lark, R. H.; Coney, L. R.; Fort, D. W.; Frasca, V.; Zurawski, V. J.; Kamen, B. A. *Cancer Res.* **1992**, *52*, 3396.
(14) Deng, Y.; Hou, Z.; Wang, L.; Cherian, C.; Wu, J.; Gangjee, A.; Matherly, L. H. *Mol. Pharmacol.* **2008**, *73*, 1274.

10.1021/cm803113e CCC: $40.75
Published on Web 03/10/2009

Scheme 1. Synthesis of Azide-Functionalized Magnetite NPs for Click Reaction

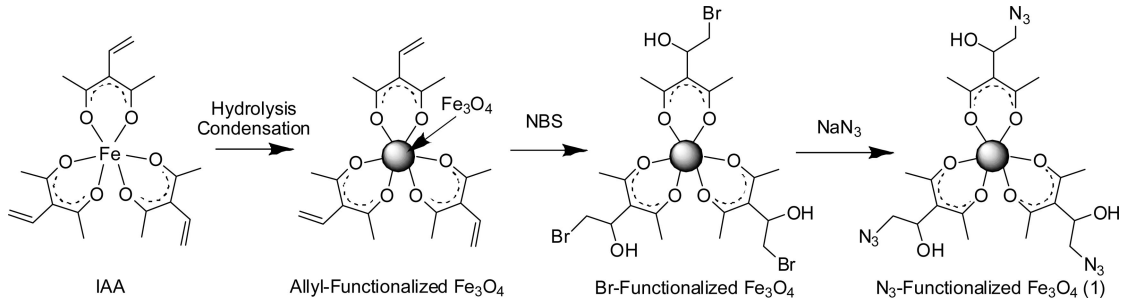

Scheme 2. Synthesis of Alkyne-Bound Folic Acid (FA) for Click Reaction

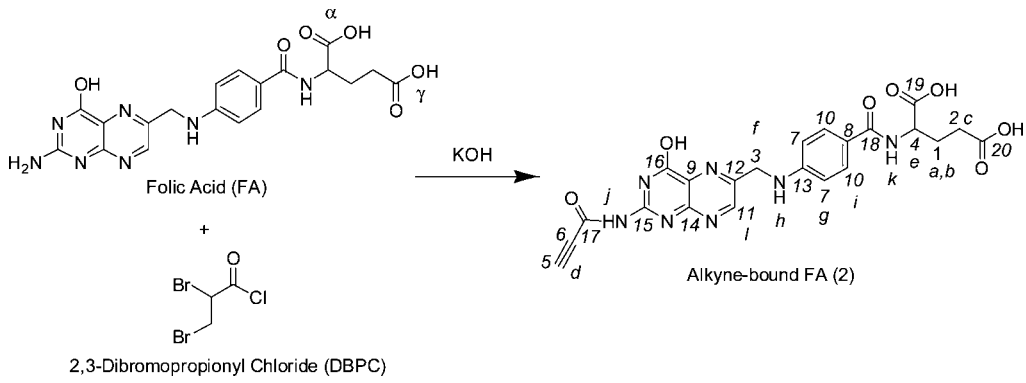

and not the γ-carboxyl group of FA (see Scheme 2, presented later in this paper) is essential for high-affinity binding to FRs on human tumors.[10,14] Therefore, the α-carboxyl group should not be modified or substituted when FA is immobilized on magnetic NPs for the delivery and accumulation in tumors. However, previous studies have overlooked the importance of the α-carboxyl group of FA. Kohler et al. reported that FA is immobilized onto magnetic NPs via the amide linkage formation between the introduced amine groups on the magnetic NPs and the α- and/or γ-carboxyl groups of FA.[15] This approach causes the loss of the α-carboxyl group of FA during the chemical modification of magnetic NPs with FA. Moreover, the intermolecular reactions between the FA molecules result in a partial loss of α-carboxyl groups, inhomogeneous FA-modification, and a reduction in the tumor-targeting ability of the complex. A novel method of chemoselective synthesis is required, by which magnetic NPs can be surface-modified with FA without the loss of the α-carboxyl group of FA.

The science of "click chemistry," introduced by Sharpless, can be used for the synthesis of drug molecules through practical and reliable reactions.[16] An example of the click reaction is the copper(I)-catalyzed variant of the Huisgen reaction, which involves 1,3-dipolar cycloaddition between azides and terminal alkynes to form 1,2,3-triazoles. The reaction has several advantages: (1) high chemoselectivity; (2) high yield with no release of byproduct; (3) no temperature or pressure control requirements; (4) easy accessibility of the two active functional groups (azide and alkyne groups) located orthogonally on the respective coupling entities; and (5) an irreversible nature that results in a stable linkage, because of the formation of a 1,2,3-triazole ring.

Magnetite (Fe_3O_4) is most commonly used as a magnetic material for biomedical applications, because it has a high saturation magnetization (~92 emu/g), a high Curie temperature (~860 K), and no cytotoxicity.[17] Fe_3O_4 NPs have been synthesized using various methods, such as coprecipitation techniques,[18] the thermal decomposition of iron compounds,[19] hydrothermal methods,[20] the reverse-micelle method,[3] and the hydrolysis of iron-organics.[21] In particular, *in situ* synthesis through the hydrolysis of iron-organics under controlled conditions allows the size of the iron oxide particles to be manipulated at the nanometer level. Furthermore, the coordination of the NPs is accomplished using the organic ligand of the precursor through the formation of chemical bonds. The organic ligand prevents agglomeration of the NPs by controlling the magnetic moment and van der Waals forces, resulting in a high dispersibility of the NPs.

This paper describes the chemoselective synthesis of folic acid-functionalized Fe_3O_4 nanoparticles (FA-Fe_3O_4 NPs) through the *in situ* hydrolysis of iron-organic compounds by applying the principles of click chemistry. We investigated the optimal conditions for the synthesis of the FA-modified Fe_3O_4 NPs and assessed the magnetic and thermal properties of these modified particles.

(15) Kohler, N.; Fryxell, G. E.; Zhang, M. *J. Am. Chem. Soc.* **2004**, *126*, 7206.
(16) Kolb, H. C.; Finn, M. G.; Sharpless, K. B. *Angew. Chem., Int. Ed.* **2001**, *40*, 2004.
(17) Chikazumi, S. *Physics of Ferromagnetism*, 2nd Edition; Oxford University Press: Oxford, U.K., 1997; p 110.
(18) Li, Z.; Tan, B.; Allix, M.; Cooper, A. I.; Rosseinsky, M. J. *Small* **2008**, *4*, 231.
(19) Sun, S.; Zeng, H. *J. Am. Chem. Soc.* **2002**, *124*, 8204.
(20) Cabañas, A.; Poliakoff, M. *J. Mater. Chem.* **2001**, *11*, 1408.
(21) (a) Yogo, T.; Nakamura, T.; Kikuta, K.; Sakamoto, W.; Hirano, S. *J. Mater. Res.* **1996**, *11*, 475. (b) Yogo, T.; Nakamura, T.; Sakamoto, W.; Hirano, S. *J. Mater. Res.* **1999**, *14*, 2855. (c) Hayashi, K.; Shimizu, T.; Asano, H.; Sakamoto, W.; Yogo, T. *J. Mater. Res.* **2008**, *23*, 3415.

Experimental Section

Materials. Iron(III) allylacetylacetonate (IAA) was prepared using the method described in the literature.[22] Ethanol (Kishida Chemical, Japan) was dried over magnesium ethoxide and then distilled before use. The following materials were used as received: hydrazine monohydrate ($N_2H_4 \cdot H_2O$), folic acid (FA), 2,3-dibromopropionyl chloride (DBPC), and *N*-bromosuccinimide (NBS), all from Tokyo Kasei (Japan); cuprous iodide (CuI), from Wako Pure Chemicals (Japan); and dimethyl sulfoxide (DMSO), potassium hydroxide (KOH), sodium azide (NaN_3), and ammonium chloride (NH_4Cl), all from Kishida Chemicals (Japan).

Allyl-Functionalized Fe_3O_4 NPs (Scheme 1). Iron(III) 3-allylacetylacetonate (IAA) (1.0 g, 2.1 mmol) was dissolved in 30 mL of ethanol. $N_2H_4 \cdot H_2O$, which serves as a reducing agent and pH adjuster (0.27 g, 8.4 mmol), and water (3.6 g, 0.2 mol) were dissolved in 10 mL of ethanol and injected into the precursor solution at 80 °C. The reaction mixture was then refluxed at 80 °C for time intervals in the range of 1.5−15 h. The solvent was removed, and the allyl-functionalized Fe_3O_4 NPs (allyl-Fe_3O_4 NPs) were obtained by drying the residue under vacuum at room temperature. Fourier transform infrared (FTIR) analysis (KBr): $\nu_s = 1639$ cm^{-1} (C═C), $\delta = 990$ and 911 cm^{-1} (alkene C−H), $\nu_s = 1584$ and 1470 cm^{-1} (coordinated diketonate ligand), and $\nu_s = 608$ and 455 cm^{-1} (spinel Fe−O).[23]

N_3-Functionalized Fe_3O_4 NPs (Scheme 1). A bromohydrin derivative was synthesized according to the methods previously described in the literature.[24] The as-synthesized allyl-Fe_3O_4 NPs were dispersed in a mixture of DMSO (10 mL) and H_2O (20 mL), and the suspension was cooled to ∼19 °C by immersing it in an ice water bath. NBS (0.415 g, 2.3 mmol) was dissolved in DMSO (10 mL) and gradually added to the cooled suspension with rapid stirring, while maintaining the temperature. The resulting suspension was stirred for 2 h to obtain a bromohydrin derivative of the allyl-Fe_3O_4 NPs. An aqueous solution of NaN_3 (0.14 g, 2.1 mmol) and NH_4Cl (0.11 g, 2.1 mmol) was added to the suspension containing the bromohydrin derivative,[16] and the mixture was heated at 80 °C for 2 h. The product, which was collected using a magnet, was washed with water and dried to obtain the N_3-functionalized Fe_3O_4 NPs (N_3−Fe_3O_4 NPs) as a solid powder. FTIR (KBr): $\nu_s = 3297$ cm^{-1} (OH), $\nu_{as} = 2080$ cm^{-1} (N═N═N), $\nu_s = 1627$ and 1529 cm^{-1} (coordinated diketonate ligand), $\delta = 1403$ and 1348 cm^{-1} (O−H), and $\nu_s = 610$ and 455 cm^{-1} (spinel Fe−O).

Alkyne-Bound FA (Scheme 2). The terminal alkyne was added to FA using the Schotten−Baumann method,[25] after which HBr was eliminated by treatment with a base.[26] FA (0.2 g, 0.45 mmol) was dissolved in a solution of KOH (0.02 g) and DMSO (30 mL). The FA solution was cooled to ∼16 °C, using an ice−water bath. DBPC (0.11 g, 0.45 mmol) was added dropwise to the FA solution, and the resultant solution was stirred at 16 °C for 2 h. It was then heated at 70 °C for 1 h, and the solvent was removed *in vacuo*. The solid thus obtained was recrystallized from a water and ethanol solution to yield an orange powder. The powder was dried under vacuum overnight. The solid thus obtained was treated with dilute hydrochloric acid (HCl) and washed with water to obtain alkyne-functionalized FA (alkyne-FA) as a solid powder. ^{1}H NMR (500 MHz, DMSO-d_6): 1.84 (m, 1H, *a*), 1.96 (m, 1H, *b*), 2.24 (t, 2H, $J = 7.4$ Hz, *c*), 2.43 (s, 1H, *d*), 4.48 (m, 1H, *e*), 4.77 (d, 2H, $J = 2.5$ Hz, *f*), 6.57 (d, 1H, $J = 8.8$ Hz, *g*), 6.87 (t, 1H, $J = 2.5$ Hz, *h*), 7.57 (d, 1H, $J = 8.8$ Hz, *i*), 8.03 (s, 1H, *j*), 8.10 (d, 1H, $J = 7.8$ Hz, *k*), and 8.68 (s, 1H, *l*).[27,28] The integral of the signal *d* was in good agreement with that of the signal *l*. ^{13}C NMR (125.7 MHz, DMSO-d_6): 26.0 (*1*), 30.5 (*2*), 45.8 (*3*), 51.8 (*4*), 55.6 (*5*), 62.3 (*6*), 111.4 (*7*), 121.4 (*8*), 128.0 (*9*), 129.0 (*10*), 148.3 (*11*), 150.7 (*12*), 151.3 (*13*), 152.9 (*14*), 159.4 (*15*), 161.0 (*16*), 166.5 (*17*), 167.5 (*18*), 173.8 (*19*), and 174.0 (*20*).[27,28] FTIR (KBr): $\nu_s = 2127$ cm^{-1} (C≡C), and $\nu_s = 1725$ cm^{-1} (C═O).[27] Anal. Calcd. for CHNO: C, 54.44; H, 3.58; N, 19.32. Found: C, 54.30; H, 3.13; N, 19.60.

Scheme 3. Synthesis of FA-Functionalized Magnetite NPs via Click Reaction

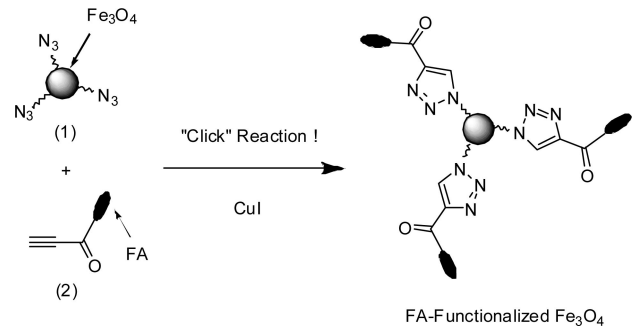

FA-Functionalized Fe_3O_4 NPs (Scheme 3). The N_3−Fe_3O_4 NPs (60 mg) and alkyne-FA (10 mg) were dissolved in a solution of DMSO (12 mL) and H_2O (4 mL). CuI was dissolved in DMSO (4 mL) and added to the above solution; the resulting mixture solution was stirred at 55 °C for 2 h. The product was collected using a magnet. The product was washed with water and dried to obtain the FA-functionalized Fe_3O_4 NPs (FA-Fe_3O_4 NPs) as a solid powder. FTIR (KBr): $\nu_s = 1710$ cm^1 (C═O), $\nu_s = 1558$ cm^1 (1,2,3-triazole),[29] $\nu_s = 1604$ and 1519 cm^{-1} (coordinated diketonate ligand), and $\nu_s = 600$ and 455 cm^{-1} (spinel Fe−O).

Characterization. The IR spectra of products were analyzed using a FTIR spectrometer (Nicolet, Nexus 470, Madison, WI). ^{1}H and ^{13}C nuclear magnetic resonance (NMR) spectra were measured with an Inova 500 spectrometer (Varian, Palo Alto, CA) in dimethylsulfoxide (DMSO)-d_6 solutions with tetramethylsilane (TMS) as the internal standard of chemical shift. The organics of the products were measured by differential thermal analysis-thermogravimetry (DTA-TG) (Model TG8120, Rigaku, Tokyo, Japan). The crystalline phases in the products were analyzed by X-ray diffraction (XRD), using Cu Kα radiation with a monochromator (Rigaku, Model RINT-2500). The crystallite size was estimated using the 311 reflection of spinel oxide, based on the Scherrer equation.[30] The particles in an organic matrix were observed by transmission electron microscopy (TEM) (Model H-800, Hitachi, Tokyo, Japan). The magnetic properties of products were measured with a vibrating sample magnetometer (VSM) (Type 5, Toei Kogyo, Tokyo, Japan) at room temperature and a superconducting quantum interference device (SQUID) (Model MPMS-7, Quantum Design, San Diego, CA) from 10 K to 300 K.

The *in vitro* hyperthermia experiments were performed using a method similar to that previously reported.[21c] To evaluate the heating properties of the product, an agar phantom dispersed with the product was subjected to an alternating current (AC) magnetic field

(22) Tayim, H. A.; Sabri, M. *Inorg. Nucl. Chem. Lett.* **1973**, *9*, 753.
(23) Tarte, P. *Comput. Rend.* **1962**, *254*, 2008.
(24) Noland, W. E., Ed. *Organic Synthesis, Collective*, *Vol. 6*; Wiley: New York, 1988; p 560.
(25) (a) Sheehan, J. C.; Bose, A. K. *J. Am. Chem. Soc.* **1951**, *73*, 1761. (b) Bose, A. K.; Mazumndar, B. N. G.; Chatterjee, B. G. *J. Am. Chem. Soc.* **1960**, *82*, 2382.
(26) Collier, W. J.; Macomber, R. S. *J. Org. Chem.* **1973**, *38*, 1367.
(27) Silverstein, R. M.; Webster, F. X.; Kiemle, D. J. *Spectrometric Identification of Organic Compounds*, 7th Edition; John Wiley & Sons: New York, 2005; p72.
(28) Bonechi, C.; Donati, A.; Lampariello, R.; Martini, S.; Picchi, M. P.; Ricci, M.; Rossi, C. *Spectrochim. Acta, Part A* **2004**, *60*, 1411.
(29) Billes, F.; Endrédi, H.; Keresztury, G. *J. Mol. Struct.* **2000**, *530*, 183.
(30) Cullity, B. D. *Elements of X-ray Diffraction*, 2nd Edition; Addison−Wesley: Reading, MA, 1978; p 284.

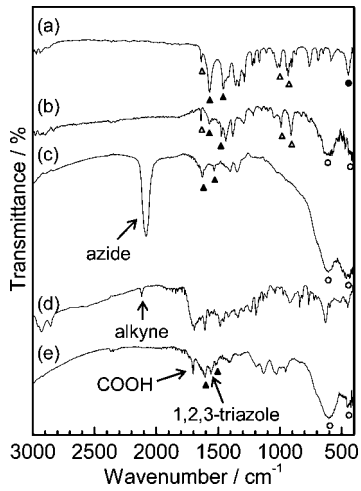

Figure 1. FTIR spectra of starting iron 3-allylacetylacetonate (spectrum (a)), allyl-Fe_3O_4 NPs (spectrum (b)), N_3−Fe_3O_4 NPs (spectrum (c)), alkyne-FA (spectrum (d)), and FA-Fe_3O_4 NPs (spectrum (e)).

with a frequency of 230 kHz and at amplitudes of 25, 50, 75, or 100 Oe, which were generated using a transistor inverter with field coils (diameter (ϕ) 120 mm × 5 turns). Agar phantom was used as simulated tissues. The phantom was spherical (ϕ = 20 mm) and consisted of agar (4%), salt (0.24%), sodium azide (0.1%), and water (95.66%). A mass of FA-modified Fe_3O_4 per milliliter of the agar phantom was 10 mg. The temperature of agar phantom was measured as a function of time using a platinel thermocouple, which was directly inserted in the phantom, under an AC magnetic field.

Results and Discussion

Synthesis of FA-Fe_3O_4 NPs. Scheme 1 summarizes the steps involved in the synthesis of N_3-functionalized Fe_3O_4 NPs. First, allyl-functionalized Fe_3O_4 (allyl-Fe_3O_4) NPs were synthesized by hydrolyzing IAA using hydrazine as the reducing agent. IAA is highly soluble in ethanol, and its allyl group is not polymerized during hydrolysis. The allyl-Fe_3O_4 NPs were converted to Br-functionalized Fe_3O_4 (Br−Fe_3O_4) NPs using NBS by introducing Br and a hydroxyl group (OH) at the terminal double bonds. Furthermore, N_3-functionalized Fe_3O_4 (N_3−Fe_3O_4) NPs were synthesized from the Br−Fe_3O_4 NPs by substituting the azide group with bromine.

Alkyne-FA was synthesized from a reaction between the amine and the carboxylic acid halide, followed by the elimination of HBr (Scheme 2). The species produced was confirmed by ^{1}H NMR, ^{13}C NMR, and FTIR (see the Experimental Section). FA-Fe_3O_4 NPs were synthesized by applying the principle of click chemistry to the reaction between N_3−Fe_3O_4 NPs and alkyne-FA (Scheme 3). The FA-functionalized Fe_3O_4 NPs that were derived from the allyl-Fe_3O_4 NPs by refluxing the reaction mixture for 1.5, 3, and 15 h have been designated as samples 1, 2, and 3, respectively.

Figure 1 shows the FTIR spectra of (a) IAA, (b) the allyl-Fe_3O_4 NPs, (c) the N_3−Fe_3O_4 NPs, (d) alkyne-FA, and (e) the FA-Fe_3O_4 NPs (sample 3). Figure 1a shows the C=C absorption band at 1630 cm^{-1} and several C=CH_2 absorptions from 995 to 900 cm^{-1} for IAA. The absorptions that are due to the diketonate ligand are denoted by solid triangles. In addition, the absorption peak for the Fe−O bond of IAA was observed at 445 cm^{-1}. When IAA was hydrolyzed at 80 °C for 15 h in the presence of hydrazine, new absorptions (marked with circles) were observed in the spectrum at 400 and 610 cm^{-1} (see Figure 1b). The bands were characteristic of the typical absorptions yielded by the spinel Fe−O. The absorptions of C=CH_2 at 1635, 990, and 911 cm^{-1} (marked with triangles) were also noticed in the spectrum of the product. This result indicates that IAA undergoes hydrolysis, resulting in the formation of iron oxide without the polymerization of double bonds. We have previously reported that IAA undergoes oligomerization when exposed to more-severe reaction conditions.[21] When IAA was reacted with a radical initiator at 80 °C for 20 h in a degassed sealed tube, the reaction yielded a mixture of trimers and hexamers; this is attributed to the reactivity of the allyl group. Monoallylic compounds do not form high-molecular-weight homopolymers in the presence of a radical initiator, because of the low reactivity of the ethylenic double bond and the high reactivity of the H atoms that are attached to the third C atom.[31] The hydrogen plays a role in degradative chain transfer, which tends to terminate chain growth.

Figure 1c shows the IR spectrum for the product obtained in the reaction between the bromohydrin derivative of allyl-Fe_3O_4 NPs and NaN_3. The absorption that is recorded at 2080 cm^{-1} reveals the presence of an azide group in the product. The spectrum obtained for alkyne-bound FA is shown in Figure 1d. The characteristic absorption of the carbon−carbon triple bond (C≡C) was observed at 2127 cm^{-1}. The data obtained by ^{1}H and ^{13}C NMR also confirmed that alkyne-substituted FA was formed. The FTIR spectrum of the FA-Fe_3O_4 NPs displayed a characteristic band corresponding to 1,2,3-triazole (1558 cm^{-1}),[29] but no bands corresponding to azide (2080 cm^{-1}) and alkyne (2127 cm^{-1}) were observed, indicating the participation of the alkyne and azide groups in the formation of 1,2,3-triazole (Figure 1d). Moreover, the stretching of the C=O bond observed at 1710 cm^{-1} is consistent with the presence of a carboxylic acid group in FA. Furthermore, the fact that the absorption bands due to the coordinated diketonate ligand (solid triangles) and Fe−O (open circles) persisted in the FA-Fe_3O_4 NP spectrum implied that the diketonated ligand was intact and attached to the particles. These results indicate that the alkyne−azide click reaction resulted in a high yield and caused the surface functionalization of Fe_3O_4 NPs with FA.

Figure 2 shows the XRD patterns of the FA-Fe_3O_4 NPs derived from allyl-FA-Fe_3O_4 NPs synthesized at 80 °C by refluxing the reaction mixture for different time intervals. The patterns shown in Figure 2 are consistent with the patterns that have been reported for bulk Fe_3O_4.[32] The crystallite sizes (D_{311}) of the Fe_3O_4 NPs formed after reflux times of 1.5, 3, and 15 h were 4.9, 6.4 and 8.0 nm, respectively, as determined using the Scherrer equation. Thus, the size of the Fe_3O_4 NPs could be controlled by adjusting the duration of reflux.

(31) Schildknecht, C. E. *Allyl Compounds and Their Polymers*; Wiley−Interscience: New York, 1973; p 1.
(32) JCPDS File Card No. No. 190629; International Centre for Diffraction Data (ICDD): Newtowne Square, PA, 1967.

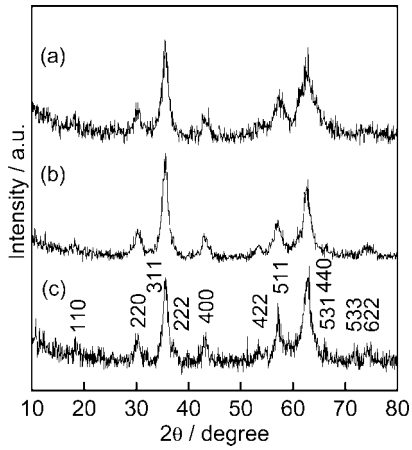

Figure 2. Change of XRD pattern of FA-Fe_3O_4 NPs with reflux time: (a) sample 1 (1.5 h), (b) sample 2 (3 h), and (c) sample 3 (15 h).

The shape and size of the products were characterized by TEM. The TEM image of sample 3 revealed that the NPs were spherical and well-dispersed (see Figure 3a). Furthermore, they had a narrow size distribution, with an average particle size of 8.2 ± 0.8 nm (relative standard deviation of 9.5%), which was slightly larger than the crystallite size determined using the Scherrer equation (see Figure 3c). Also, the size of NPs increased as the reflux time increased; the mean size of samples 1, 2, and 3 were 5.0, 6.6, and 8.2 nm, respectively (see Figure S1 in the Supporting Information and Figure 3a in this paper). In addition, the selected area electron diffraction (SAED) pattern for sample 3, which consisted of spots on the rings, revealed that the NPs were crystalline (see Figure 3b). The *d*-values of the SAED were very consistent with those obtained for Fe_3O_4.[32]

TGA revealed that the organic contents of the allyl-Fe_3O_4 NPs synthesized by refluxing the reaction mixture for 1.5, 3, and 15 h were 15, 14, and 13 wt %, respectively. The amounts of organic phase for samples 1, 2, and 3 were also 24, 23, and 22 wt %, respectively. The organics of FA-Fe_3O_4 NPs increased, compared to those before functionalization. Assuming that the density of the Fe_3O_4 NPs in sample 3 was equivalent to the bulk density (i.e., 4.8 g/cm^3), and that the NPs were spherical, we estimated that ~392 molecules were associated with each NP.

Magnetic Properties of the FA-Fe_3O_4 NPs. Figure 4 shows the $M-H$ curves plotted for samples 1, 2, and 3 measured at room temperature. The magnetization values (M) of samples 1, 2, and 3 at 16 kOe were 42, 51, and 57 emu/g, respectively. Because TGA revealed the inorganic contents of samples 1, 2, and 3 to be 76, 77, and 78 wt %, respectively, the corrected magnetization values (M_C) at 16 kOe were determined to be 55, 66, and 73 emu/g, respectively. These M_C values respectively correspond to 60%, 72%, and 79% of the values obtained for bulk Fe_3O_4 (92 emu/g), measured at room temperature.[17] The M and M_C values for sample 3 at 16 kOe were determined to be higher than the corresponding values reported for similarly sized Fe_3O_4 NPs (M = 21 emu/g, M_C = 57 emu/g; 8.5-nm Fe_3O_4 NPs).[18] Also, the M values of allyl-Fe_3O_4 NPs synthesized by refluxing the reaction mixture for 1.5, 3, and 15 h were 47, 52, and 55 emu/g, respectively. The M_C values for those NPs were 55, 60, and 63 emu/g, and those values correspond

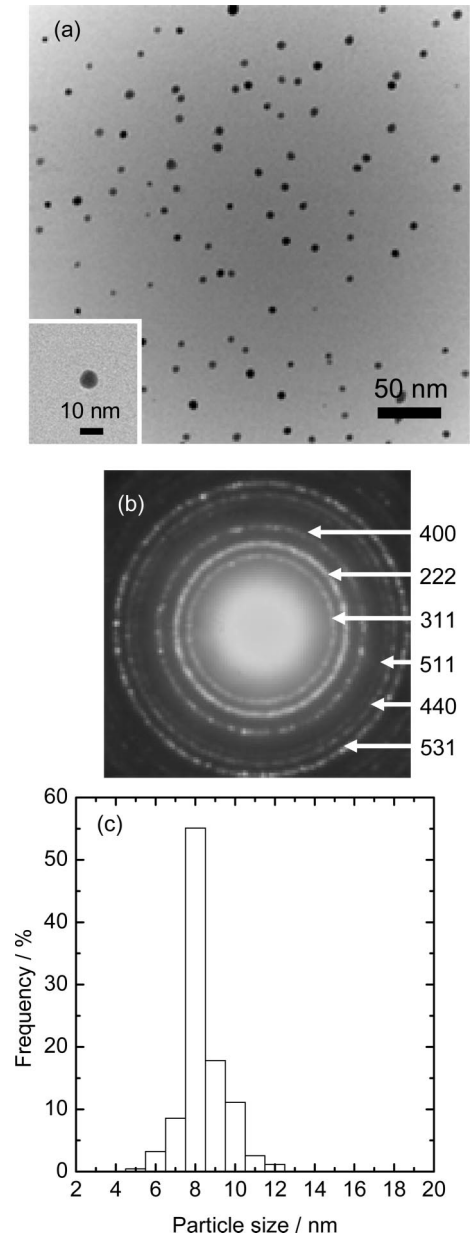

Figure 3. Microstructure of FA-Fe_3O_4 NPs synthesized at 80 °C for 15 h (sample 3), (a) TEM image,(b) SAED, and (c) particle size distribution.

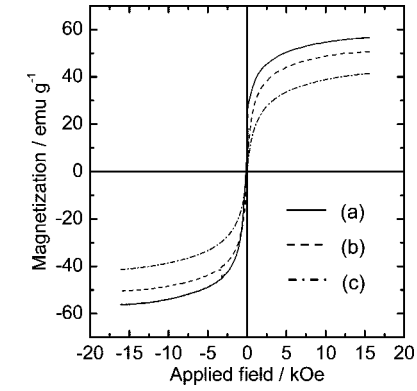

Figure 4. Magnetization versus magnetic field ($M-H$) curves for FA-Fe_3O_4 NPs at room temperature: (a) sample 3 (curve (a)), sample 2 (curve (b)), and sample 1 (curve (c)).

to 59%, 65%, and 68% of the value for bulk Fe_3O_4, respectively. Thus, the M_C values after functionalization are

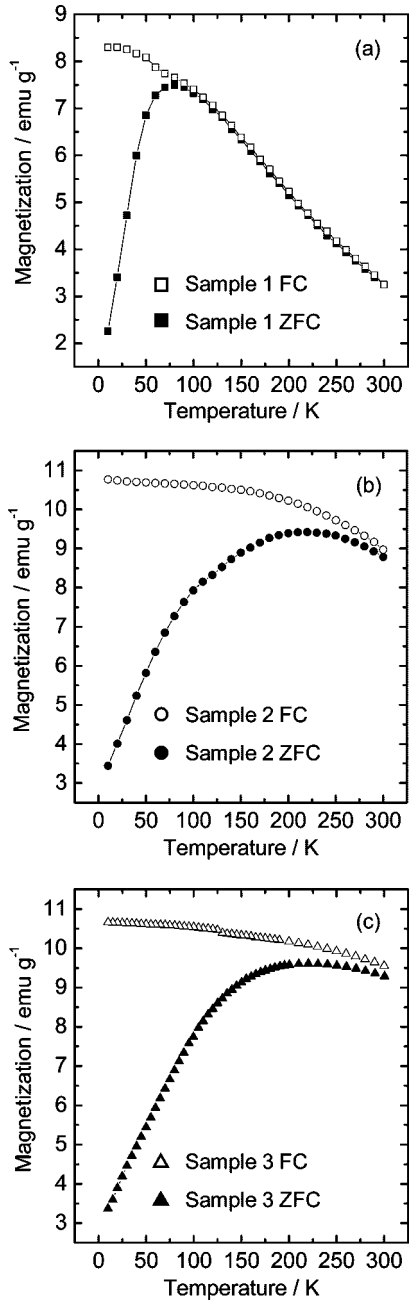

Figure 5. Temperature dependence of magnetization of FA-Fe_3O_4 NPs at 100 Oe: (a) sample 1 (1.5 h), (b) sample 2 (3 h), and (c) sample 3 (15 h). (Open symbols denote FC samples, and solid symbols denote ZFC samples.)

higher than those before functionalization. The repeated heat treatments during functionalization increase the surface crystallinity of NPs, which enhances the saturation magnetization of NPs.

Figure 5 shows the zero-field cooling (ZFC) and the field cooling (FC) curves plotted for samples 1, 2, and 3 from 300 K to 10 K at 100 Oe. The magnetization of the FC curves increases monotonously as the temperature decreases. In contrast, the magnetization of the ZFC curves initially increases as the temperature decreases, reaching a maxima, and then decreases once again with an additional decrease in temperature. The blocking temperature (T_B) is denoted by the cusp of the ZFC curves. The T_B temperatures for samples 1, 2, and 3 are 80, 220, and 240 K, respectively. According to Néel's theory, the T_B temperature of a single domain particle is related to the particle volume (V) and the magnetic anisotropy constant (K_a), using the following relationship:

$$K_a = \frac{25 k_B T_B}{V} \tag{1}$$

where k_B is the Boltzmann constant. The K_a values for samples 1, 2, and 3 were estimated to be 4.2×10^5, 3.6×10^5, and 2.3×10^5 J/m^3, respectively; these values were higher than that obtained for bulk Fe_3O_4 ($1.1-1.3 \times 10^4$ J/m^3).[33] The K_a value for magnetic NPs increases as the particle size decreases,[34] because the spin disorder on the NP surface causes a reduction in the magnetic moment. The K_a value is reflective of the difference in the thickness of the defective surface layer of the NPs and indicates that the defective surface layer of sample 3 is relatively thin.

Figure 6 shows the magnetization curve of sample 3, measured at temperatures of <300 K. Remanence and coercivity were not observed in either of the corresponding curves at 250 and 300 K. The magnetization at 250 K is higher than that at 300 K (see Figure 6a). The magnetization observed in magnetic NPs is explained by the Langevin equation:

$$\frac{M}{M_S} = \coth\left(\frac{\mu H}{k_B T}\right) - \left(\frac{k_B T}{\mu H}\right) \tag{2}$$

where M_S is the saturation magnetization, H the magnetic field, T the absolute temperature, and μ the magnetic moment.[35] The magnetization of sample 3 at 250 and 300 K was plotted as a function of H/T; the data for both temperature conditions are superimposed in Figure 6b. Thus, the plots for values measured at >250 K satisfy the Langevin function. Below T_B, the $M-H$ curves of sample 3 exhibit coercivity and remanence: their values are 55 Oe and 3.5 emu/g at 100 K, and 450 Oe and 19 emu/g at 10 K, respectively (Figure 6c). The results shown in Figure 6a−c confirm that sample 3 has superparamagnetic properties. Furthermore, because samples 1 and 2 have smaller particle sizes than that of sample 3, the former two samples are also superparamagnetic. According to the Langevin equation, the diameter of the Fe_3O_4 particles can be calculated by the following equation:

$$\frac{M}{M_S} = \frac{\nu H}{3 k_B T} \tag{3}$$

where ν is the volume of the Fe_3O_4 particles. The particle size estimated using eq 3 was 8.0 nm; this value was consistent with that obtained by XRD and TEM. The correlation between these results demonstrates good crystallinity of the Fe_3O_4 NPs, which renders them highly magnetic.

(33) Goya, G. F.; Berquó, T. S.; Fonseca, F. C.; Morales, M. P. *J. Appl. Phys.* **2003**, *94*, 3520.
(34) Park, J.; An, K.; Hwang, Y.; Park, J. G.; Noh, H. J.; Kim, J. Y.; Park, J. H.; Hwang, N. M.; Heyon, T. *Nat. Mater.* **2004**, *3*, 891.
(35) Morrish, A. H. *The Physical Principles of Magnetism*; John Wiley & Sons: New York, 1965; p 360.

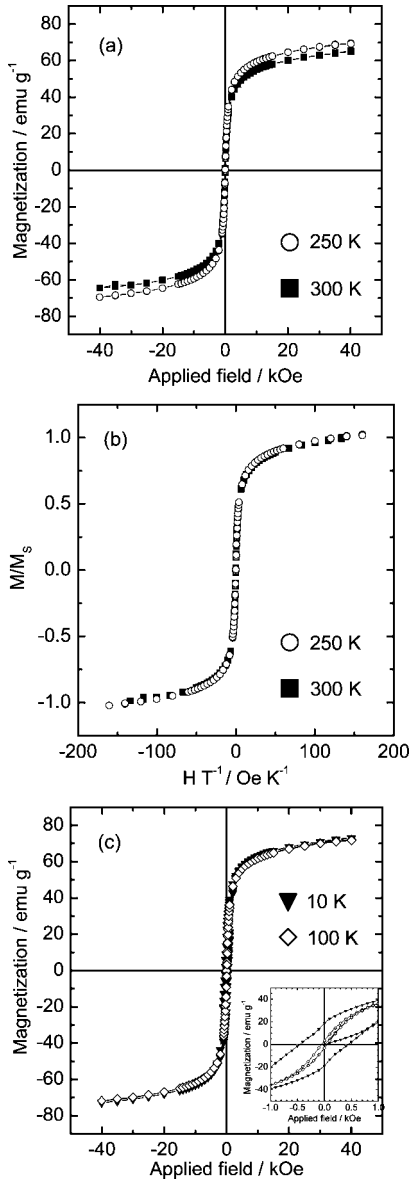

Figure 6. (a) Magnetization versus field ($M-H$) curves of sample 3 at 250 and 300 K. (b) Field versus temperature (H/T) superposition of isothermal magnetization data from 250 K to 300 K. (c) $M-H$ curves of sample 3 at 10 and 100 K; inset shows loops at lower magnetic field.

Heating Properties of FA-Fe_3O_4 NPs. The exothermic behavior exhibited by superparamagnetic materials under the effect of an AC magnetic field is primarily due to Néel relaxation.[4] The heat generated is assessed in terms of the specific absorption rate (SAR), which is denoted as the specific loss power, to compare the efficiency of different samples.[4] The SAR is defined as follows:

$$\mathrm{SAR} = C\left(\frac{\mathrm{d}T}{\mathrm{d}t}\right)\left(\frac{m_\mathrm{a}}{m_\mathrm{m}}\right) \tag{4}$$

where C is the specific heat capacity of the agar phantom (4.186 J g^{-1} °C^{-1}), dT/dt the initial slope of the temperature change versus time dependence, m_a the mass of the agar phantom that contains the FA-Fe_3O_4 NPs, and m_m the mass of the Fe_3O_4 NPs in the agar phantom.

Figure 7a shows the temperature change versus time for the agar phantoms that contain samples 1, 2, and 3. The

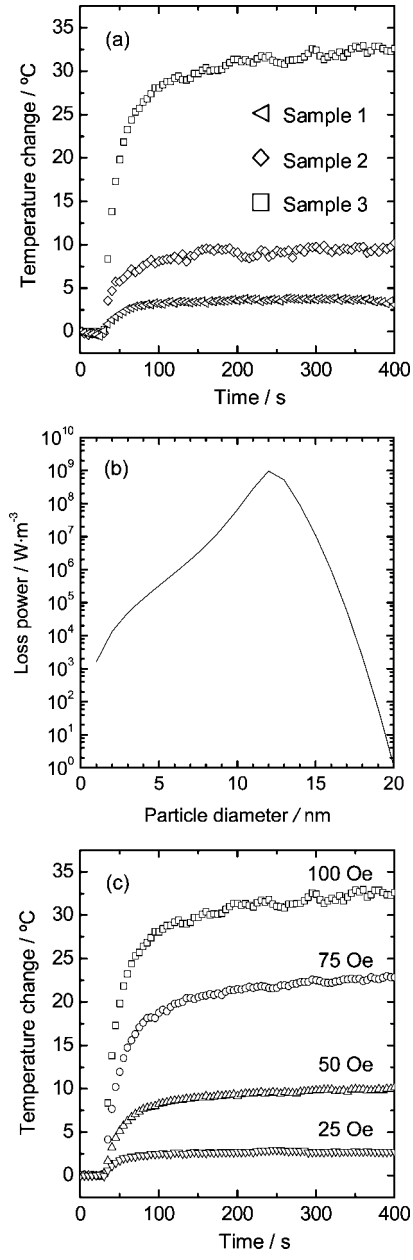

Figure 7. (a) Temperature change of the spherical agar phantom dispersed with 10 mg/mL of samples 1, 2, and 3 under a 230 kHz AC magnetic field and 100 Oe. (b, c) Temperature change of the spherical agar phantom dispersed with 10 mg/mL of sample 3 under a 230-kHz AC field from 25 Oe to 100 Oe.

frequency was 230 kHz, and the magnetic field amplitude was 100 Oe. The SAR values determined for samples 1, 2, and 3 are 36, 102, and 670 W/g, respectively. The temperature change and SAR value drastically increases as the particle size increases from 4.9 nm (sample 1) to 8.0 nm (sample 3). The relaxation loss P at temperature T, as determined in terms of the magnetic relaxation time τ, is evaluated using the following equations:[36]

$$P = \frac{V(M_\mathrm{S}H\omega\tau)^2}{2\tau k_\mathrm{B}T(1+\omega^2\tau^2)} \tag{5}$$

where M_S is the saturation magnetization of Fe_3O_4, V is the volume of the particles, k_B is the Boltzmann constant; and H and ω are the amplitude and angular frequency of the AC magnetic field. In addition,

$$\frac{1}{\tau} = \frac{1}{\tau_N} + \frac{1}{\tau_B} \cong \frac{1}{\tau_N} = \frac{2\sqrt{\frac{KV}{kT}}}{\sqrt{\pi}\tau_0 \exp\left(\frac{KV}{kT}\right)} \quad (6)$$

where τ_N is the Néel relaxation time, τ_B the Brownian relaxation time, K the anisotropy constant, and τ_0 the relaxation factor. Figure 7b shows the loss power due to Néel relaxation for the Fe_3O_4 NPs; the values were calculated from eq 5, as a function of the particle size d. The power loss was determined to be optimum at a particle size of 12 nm. The power-loss values for the 6.4-nm and 8.0-nm Fe_3O_4 NPs were, respectively, ~4 and ~20 times larger than that of the 4.9-nm Fe_3O_4 NPs. These results explain the dramatic increase in the SAR value with an increase in the particle size from 6.4 nm to 8.0 nm (see Figure 7a). Moreover, the SAR values measured for samples 1, 2, and 3 at 230 kHz and 100 Oe were significantly higher than the reported values; this is either because (i) the temperature increased rapidly under the influence of an applied magnetic field or (ii) the initial slope was steep. Drake et al. reported that a temperature change of 12 °C over 50 min yields a SAR value of 115 W/g at 1 MHz and 100 Oe.[37]

In the case of sample 3, the temperature increases as the amplitude of the applied magnetic field increases from 25 Oe to 100 Oe (Figure 7c). The SAR values recorded at 25, 50, 75, and 100 Oe were 33, 131, 348, and 670 W/g, respectively. Fortin et al. reported a high SAR value (i.e., 1650 W/g) for a suspension of γ-Fe_2O_3,[38] in the presence of a 700-kHz AC magnetic field at 310 Oe; the amplitude applied in their study was much higher than that applied in the present one. The SAR value is proportional to the frequency and the square of the amplitude of the magnetic field;[39] given this information, the SAR values obtained in the present study were quite high for the applied frequency and amplitude. This result can be attributed to the high saturation magnetization and the thin shell layer of the Fe_3O_4 NPs. The high magnetization of the samples translates to an excellent heating ability. Moreover, for biological applications, NPs should be able to achieve a temperature gain of more than 6.5 °C because the normal body temperature is ~37 °C, and the threshold temperature for hyperthermia is 42.5 °C. A relatively low amplitude (in the range of 25−50 Oe) was sufficient to cause the required increase in temperature (see Figure 7c).

Conclusions

We achieved the chemoselective synthesis of folic acid-functionalized Fe_3O_4 nanoparticles (FA-Fe_3O_4 NPs) by applying *in situ* hydrolysis and condensation, along with the principle of "click chemistry"; the functionalization was achieved without loss of the α-carboxylic acid groups of folic acid (FA). The terminal double bond of iron(III) allylacetylacetonate (IAA) was used for further chemical modification. Among the Fe_3O_4NPs, Fe_3O_4 NPs were monodisperse and their particles possessed high magnetization and could achieve an adequate increase in temperature. Under the influence of a minimal magnetic field, these NPs can achieve an adequate temperature gain, so that, if used for biological applications, they can raise the body temperature to the threshold level for hyperthermia treatment. In addition, the FA-Fe_3O_4 NPs are expected to possess an effective tumor-targeting ability because the free α-carboxylic acid groups in FA exhibit high affinity for folate receptors (FRs) on tumor cells. The immobilization of FA on magnetic particles without the loss of the α-carboxylic acid groups resulted in the formation of multifunctional nanoparticles that are useful for biomedical applications.

Supporting Information Available: Figure S1 shows TEM images of (a) sample 1 (1.5 h) and (b) sample 2 (3 h). This material is available free of charge via the Internet at http://pubs.acs.org.

CM803113E

(36) (a) Rosensweig, R. E. *J. Magn. Magn. Mater.* **2002**, *252*, 370. (b) Okawa, K.; Sekine, M.; Maeda, M.; Tada, M.; Abe, M.; Matsushita, N.; Nishio, K.; Handa, H. *J. Appl. Phys.* **2006**, *99*,08H102.
(37) Drake, P.; Cho, H. J.; Shih, P. S.; Kao, C. H.; Lee, K. F.; Kuo, C. H.; Lin, X. Z.; Lin, Y. J. *J. Mater. Chem.* **2007**, *17*, 4914.
(38) Fortin, J. P.; Wilhelm, C.; Servais, J.; Ménager, C.; Bacri, J. C.; Gazeau, F. *J. Am. Chem. Soc.* **2007**, *129*, 2628.
(39) Hiergeist, R.; Andrä, W.; Buske, N.; Hergt, R.; Hilger, I.; Richter, U.; Kaiser, W. *J. Magn. Magn. Mater.* **1999**, *201*, 420.